Short communication

A high-performance reversible protonic ceramic electrochemical cell based on a novel Sm-doped $BaCe_{0.7}Zr_{0.1}Y_{0.2}O_{3-\delta}$ electrolyte

Yuqing Meng, Jun Gao, Hua Huang, Minda Zou, Jack Duffy, Jianhua Tong, Kyle S. Brinkman[*]

Department of Materials Science and Engineering, Clemson University, Clemson, SC, 29634, USA

HIGHLIGHTS

- Utilized Sm-doping to enhance processing and improve proton conductivity.
- Tested cells in protonic fuel cell (PCFC) and electrolysis cell (PCEC) operation.
- Maximum power density of 410 $mWcm^{-2}$ is observed in PCFC at 600 °C.
- Current density of 370 $mAcm^{-2}$ with an applied voltage of 1.3 V in PCEC mode.

ABSTRACT

The present work describes a doping strategy to improve the electrochemical performance of $BaCe(Zr)O_3$-based reversible protonic ceramic electrochemical cells (RePCECs). $BaCe_{0.7}Zr_{0.1}Y_{0.2-x}Sm_xO_{3-\delta}$ ($0 \leq x \leq 0.2$) synthesized by a solid-state reactive sintering method. Enhanced sintering with Sm-doping is observed with a significant increase of grain size as compared to un-doped samples. The improvement of the proton conductivity by proper Sm-doping is also achieved. This work fabricates and tests an electrochemical cell with a 25 μm thick electrolyte in both protonic ceramic fuel cell (PCFC) and protonic ceramic electrolysis cell (PCEC) operation modes. At the intermediate temperature of 600 °C, a maximum power density of 410 $mWcm^{-2}$ is observed in PCFC mode under Air/H_2 gradient, while a current density of 370 $mAcm^{-2}$ is obtained with an applied voltage of 1.3 V in PCEC mode using 12 vol% H_2O humidified air as feed gas and 5% H_2 as sweep gas.

1. Introduction

A reversible protonic ceramic electrochemical cell (RePCEC) is a ceramic energy device that can operate both in fuel cell and electrolysis modes, using proton-conducting ceramic as an electrolyte. Compared to other reversible electrochemical cells, such as low-temperature proton exchange membrane fuel cells (PEMFCs), high-temperature solid oxide fuel cells (HT-SOFCs) and high-temperature solid oxide electrolysis cells (HT-SOFCs), RePCECs can provide several unique advantages including the production of pure dry hydrogen [1–5], higher efficiency [6], broad fuel flexibility [1], long-term durability [6], and low-cost [7]. The current state-of-the-art RePCEC electrolytes are $BaCeO_3$ and $BaZrO_3$-based materials [8–13]. $BaZrO_3$-based proton conductors possess relatively low conductivity but exhibit exceptional stability to water and carbon dioxide. In contrast, $BaCeO_3$-based electrolytes exhibit higher proton conductivity, which is closely correlated with doped trivalent elements. Yttrium doped barium cerate and zirconate of $BaCe_{0.7}Zr_{0.1}Y_{0.2}O_{3-\delta}$

(BCZY) is a promising electrolyte which has both excellent chemical stability and proton conductivity [14]. The replacement of cerium or zirconium by a trivalent cation (i.e., Gd, Y, Sm) will introduce oxygen vacancies into the perovskite structure resulting in enhanced proton concentration in these materials. Good cell performance could be obtained by choosing appropriate dopant and control the doping level.

Samarium is widely used a dopant in ceria-based materials to improve ionic conductivity, and the critical dopant concentration to achieve total conductivity was reported to be approximately 20 mol% [15,16]. Iwahara [17] found that Sm-doped $BaCeO_3$ is a pure proton conductor in hydrogen atmosphere below 700 °C. Gorbova et al. [18] reported that the sintering ability as well as the grain size of $BaCe_{0.8}Y_{0.2}O_{3-\delta}$ can be improved by Sm-doping, which agrees with the result reported by Shi et al. [11] It is generally recognized that the lower distortion of the lattice cell and larger free volume favor the ionic conduction in perovskites [19]. According to the definition of Goldschmidt tolerance factor (*t*) and free volume (V_f), replacement of Y^{3+} (1.019 Å)

by Sm^{3+} (1.079 Å) increases the lattice distortion while enlarging the free volume. In addition, the relatively lower average metal-oxygen bond energy of Sm-doped BCZY is favor of oxygen migration (Sm–O, 573 kJmol^{-1}, Y–O, 714.1 ± 10.2 kJmol^{-1}). Hence, a proper doping level of Sm is expected to balance the contradictory contribution and exhibit improved conductivity and chemical stability.

Proton conducting ceramic electrolytes may contain large grain boundary contributions, meaning that the conductivity of poly-crystalline samples is generally significantly lower than the corresponding bulk (grain interior) conductivity [20–23]. The properties of the grain boundary are known to be strongly affected by the material processing conditions, therefore both the microstructure as well as the materials compositions require optimization. An additional potential benefit of Sm doping is the ability for enhanced sintering of Sm doped $BaCeO_3$-based proton conductor, leading to a larger grain size and reduced interfacial contribution [11].

In the present study, the perovskite-type oxide solid solutions $BaCe_{0.7}Zr_{0.1}Y_{0.2-x}Sm_xO_{3-\delta}$ (with $0 \leq x \leq 0.2$) were synthesized using solid state reactive sintering (SSRS) method. The effect of microstructure and composition on the total conductivity (bulk conductivity and grain boundary conductivity) was studied. Single cells with the optimized electrolyte composition and microstructure were measured in both fuel cell and electrolysis cell mode.

2. Experimental

2.1. Preparation of BCZYSm pellets

Proton conducting ceramic pellets of $BaCe_{0.7}Zr_{0.1}Y_{0.2-x}Sm_xO_{3-\delta}$ (denote as BCZYSm, x = 0.0, 0.05, 0.07, 0.09, 0.10, 0.11, 0.13, 0.15, 0.20) were synthesized by the SSRS method [24,25] from cost-effective raw materials of $BaCO_3$ (Alfa Aesar, 99.8%), CeO_2 (Alfa Aesar, 99.9%), ZrO_2 (Alfa Aesar, 99.7%), Y_2O_3 (Alfa Aesar, 99.9%), Sm_2O_3 (Alfa Aesar, 99.9%) and NiO (Baker Analyzed Reagent, 99.0%). Stoichiometric amounts of $BaCO_3$, ZrO_2, CeO_2, Y_2O_3 and Sm_2O_3 were weighted and added into a Nalgene bottle. 1.0 wt% sintering aid of NiO (based on the total weight of precursor mixer) was added into the above powder mixture. The resulted precursor slurry was ball milled with ethanol (Carolina, 95%) solvent and 12.5 mm diameter spherical alumina grinding media (Inframat Advanced Materials) for 24 h, then dried at 80 °C for 48 h. Pellets with a diameter of 15 mm was then fabricated by uniaxial pressing under 300 MPa pressure for a dwell of 2 min, followed by sintering at 1400 °C for 18 h in ambient air.

2.2. Preparation of single cell component precursors

The precursor of the H_2 electrode with a nominal composition of 40 wt% BCZYSm +60 wt% NiO was prepared by mixing proper amounts of $BaCO_3$, ZrO_2, CeO_2, Y_2O_3, Sm_2O_3 and NiO according to the desired stoichiometry and 25 wt% (based on total weight of oxides and carbonates raw materials) starch as pore former. The precursor of the $BaCe_{0.6}Zr_{0.3}Y_{0.1}O_{3-\delta}$ (BCZY63) O_2 electrode scaffold was prepared by mixing proper amounts of $BaCO_3$, ZrO_2, CeO_2 and Y_2O_3 according to the desired stoichiometry with 0.025 wt% Fe_2O_3 as a sintering aid and 45 wt% starch as pore-former. This precursor powder was ball-milled in ethanol with 3 mm YSZ beads for 24 h, followed by drying at 90 °C for 24 h. The precursor of BCZYSm electrolyte was prepared followed the same procedure described in section 2.1. The electrolyte and O_2 electrode scaffold were prepared by mixing the respective precursor powders with dispersant (20 wt% solsperse 28000 dissolved in terpinol) and binder (5 wt% V-006 (Heraeus) dissolved in terpinol), with a ratio of 15:3:1.

The precursor solution of the $BaCo_{0.4}Fe_{0.4}Zr_{0.1}Y_{0.1}O_{3-\delta}$ (BCFZY0.1) active O_2 electrode nanoparticles was prepared as following procedure. Stoichiometric amounts of $Ba(NO_3)_2$ (Alfa Aesar, 99+%), Co $(NO_3)_2\cdot6H_2O$ (Alfa Aesar, >98.0%), $Fe(NO_3)_3\cdot9H_2O$ (Alfa Aesar,
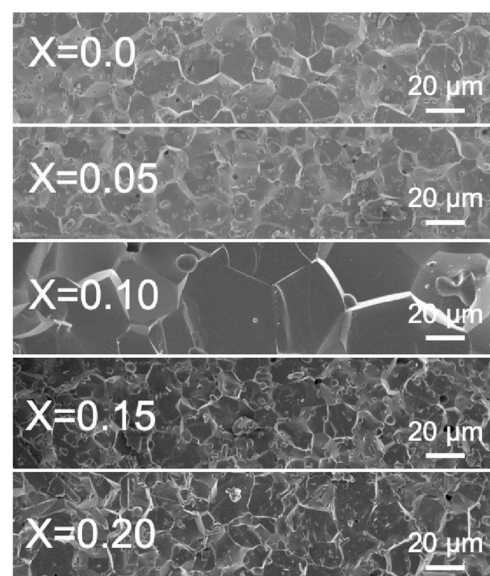

Fig. 1. SEM images of $BaCe_{0.7}Zr_{0.1}Y_{0.2-x}Sm_xO_{3-\delta}$ (denote as BCZYSm, x = 0.0, 0.05, 010, 0.15, 0.20) with NiO as sintering aid sintered at 1400 °C for 18 h.

>98.0%), $ZrO(NO_3)_2$ solution (Sigma-Aldrich, ≥99%) and Y $(NO_3)_3\cdot6H_2O$ (Alfa Aesar, 99.9%) were dissolved in distilled water in correct molar ratios, then mixing with citric acid (Sigma-Aldrich, ≥99.5%) to produce a solution with a citric acid/metal-ion ratio of 1.5:1.

2.3. Fabrication of single cells

The H_2 electrode precursor powder was dry-pressed under 350 Mpa for 2 min in a circular die set with a diameter of 19 mm to produce green H_2 electrode pellets. Then a thin electrolyte precursor paste layer (20–30 μm after firing) was deposited on both sides of the green H_2 electrode precursor pellets using screen-printing. Then the O_2 electrode scaffold precursor paste layer was subsequently coated on top of one of the electrolyte layers. The overall structure was heated to 1400 °C for 18 h followed by removal of the extra electrolyte by a grinding step. The BCFZY0.1 solution was infiltrated into the pores of the O_2 electrode scaffold structure using a microliter to control the loading amount. The infiltrated cells were fired at 400 °C for 1 h. This procedure was repeated until the desired weight loading of BCFZY0.1 was achieved. Finally, the single cells were heated in air to 900 °C for 5 h to produce the nano crystalline perovskite structure of BCFZY0.1.

2.4. Characterization

The crystal structure of the BCZYSm samples was examined using X-ray diffraction (XRD, Rigaku TTR-III diffractometer) with Cu *Kα* radiation source. The XRD patterns were obtained in the range of 20°–80° with a 0.02° step size and a scan speed of 0.5°min^{-1}. The microstructure of dense pellets and single cells were examined using scanning electron microscopy (SEM, Hitachi S-4800). The density of the samples was measured using Archimedes method.

The as-fabricated single cells were sealed in an aluminum tube by ceramic bond, using silver wires as the voltage and current leads on both sides. The electrochemical performance of single cells in fuel cell mode was evaluated by using the humidified hydrogen (3 vol% H_2O) as the fuel and the ambient air as oxidant. The electrolysis cell mode was then evaluated with humidified air (12% H_2O) [26] steam fed in the air electrode and humidified hydrogen (3 vol% H_2O) fed into the hydrogen electrode. The flow rates of fuel and oxidant were set to be 50 and 150 ml/min, respectively.
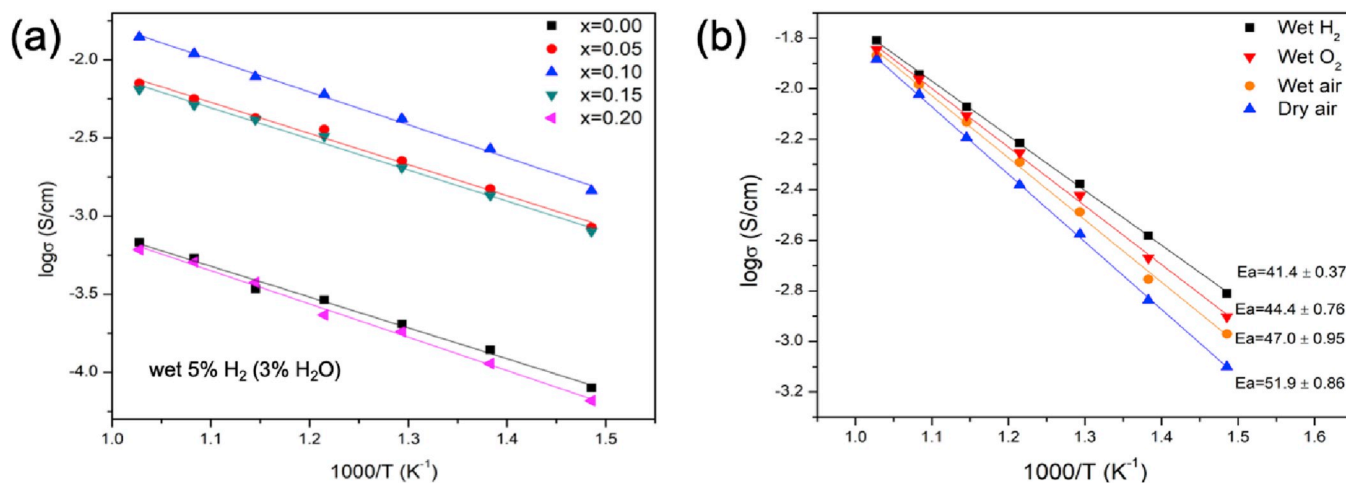
Fig. 2. (a) Electrical conductivities of $BaCe_{0.7}Zr_{0.1}Y_{0.2-x}Sm_xO_{3-\delta}$ (x = 0, 0.05, 0.10, 0.15, 0.20) as measured at 400–700 °C in wet 5% H_2 (with ~3 vol % H_2O), and (b) Arrhenius plot of BCZYSm10 in various environments at temperature range 400–700 °C.

3. Results and discussion

3.1. Microstructure of BCZYSm electrolyte pellets

The scanning electron microscopy (SEM) micrographs of fractured cross section of as-sintered BCZYSm pellets are presented in Fig. 1. The cross sections of all the BCZYSm pellets appear dense with negligible amount of pores. The fractured locations for all the samples are along the grain boundaries. The grain sizes obtained here for BCZYSm with x = 0.0, 0.05, 0.15 and 0.20 are similar to those reported in the literature for typical yttrium-doped barium cerate [27]. A much larger grain size was observed for the pellet with 10% Sm dopant. The X-ray diffraction patterns of the as-prepared BCZYSm pellets are displayed in Fig. S1. The patterns reveal that the diffraction peaks obtained for each sample can

be indexed on the basis of an orthorhombic perovskite structure (space group Pmnb). A slight peak shift to the lower-angle region indicated the lattice expansion with Sm doping. A further XRD refinement (Fig. S2) shows that an increase of lattice parameter a and c with increase of Sm doping level, while b axis keeps constant (Fig. S3).

3.2. Electrical conductivity of BCZYSm electrolyte pellets

Fig. 2a reveals the Arrhenius plot of the electrical conductivity of $BaCe_{0.7}Zr_{0.1}Y_{0.2-x}Sm_xO_{3-\delta}$ in wet 5% H_2. The conductivity first increased Sm content until x = 0.10, with a total conductivity of 7.94×10^{-3} Scm^{-1} for $BaCe_{0.7}Zr_{0.1}Y_{0.1}Sm_{0.1}O_{3-\delta}$ at 600 °C. At higher Sm content levels, the total conductivity started to decrease. The total conductivity varied with x according to the following sequence: 0.10 > 0.05 >
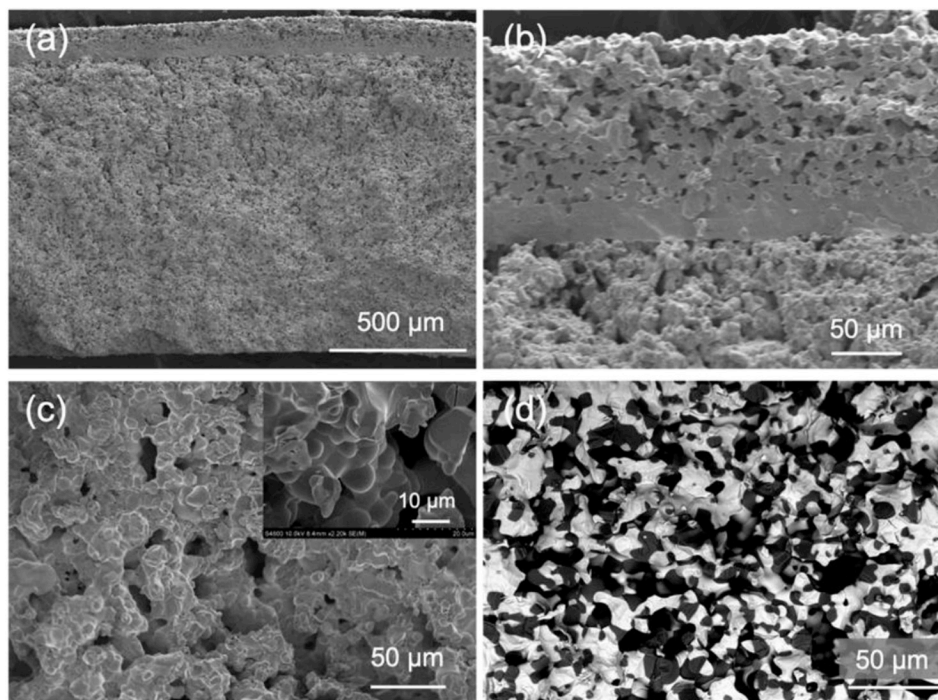

Fig. 3. (a) A cross-sectional view of a cell with configuration of Ni-BCZYSm10| BCZYSm10 |BCZY63-BCFZY0.1, (b) enlarged view of electrolyte, (c) microstructure of anode after reducing under 5% H_2 at 600 °C for 24 h (inset is the enlarged view of anode particles), and (d) SEM BSE image of reduced anode (bright and dark phases correspond to Ni and BCZYSm10, respectively).
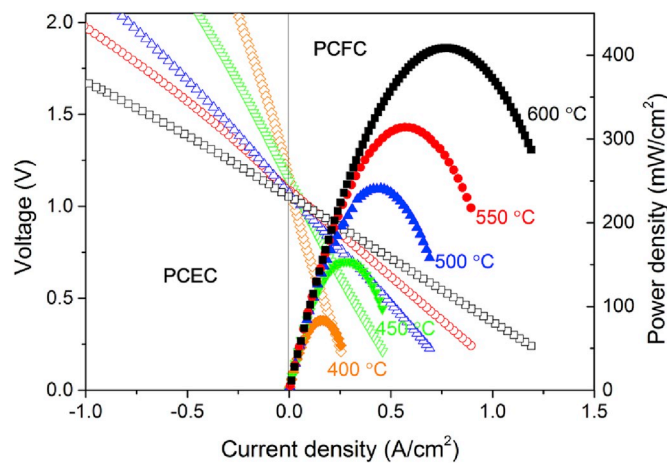
Fig. 4. (a) I–V curves and corresponding power densities of 40 wt% BCZYSm10 + 60 wt% NiO | BCZYSm10 | BCZY63 + BCFZY0.1 cell at 400–600 °C under PCFC working mode under H_2/air atmosphere, and electrolysis performance measured under 12 vol% H_2O humidified air/wet H_2 (cathode area: 0.38 cm²), (b) Impedance spectra of single cell in the temperature range at 550 °C and 600 °C (raw impedance data was multiplied by the fuel cell effective area).

0.15 > 0.00 > 0.20. The enhanced impact of Sm-doping on the electrical conductivity of BaCeO₃-based materials was also reported by Amisf et al. [28]. More specific Sm concentration shown in Fig. S5 manifests that $BaCe_{0.7}Zr_{0.1}Y_{0.1}Sm_{0.1}O_{3-\delta}$ has a highest conductivity in wet H_2. The typical impedance spectrum of $BaCe_{0.7}Zr_{0.1}Y_{0.2-x}Sm_xO_{3-\delta}$ (x = 0.07, 0.09, 0.10, 0.11) samples were fitted according to the equivalent circuit (Fig. S6a). It is conspicuous that the grain boundary conductivity is lower than the bulk conductivity by more than one order of magnitude (Fig. S6b). Both the bulk conductivity (σ_b) and grain boundary conductivity (σ_{gb}) increased with Sm content, reaching a maximum at x = 0.10 followed by a subsequent decrease at higher Sm doping levels. The increased σ_b with Sm content up to x = 0.10 was ascribed to the increasing grain size (Fig. S4) [29].

Fig. 2b shows the electrical conductivities of BCZYSm10 in four different atmospheres. BCZYSm10 may possess protonic, oxygen-ionic and mixed ionic and electronic transport properties, depending on the temperature and atmospheres [30]. Oxygen vacancies can be created by acceptor doing (Equation (1)). Meanwhile, the p-type electronic conductivity also appears when oxygen molecules are incorporated into the lattice (Equation (2)).
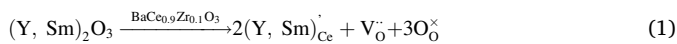
$$(Y, Sm)_2O_3 \xrightarrow{BaCe_{0.9}Zr_{0.1}O_3} 2(Y, Sm)'_{Ce} + V^{\bullet\bullet}_O + 3O^\times_O \tag{1}$$

$$O_2 + 2V^{\bullet\bullet}_O \rightarrow 2O^\times_O + 4h^\bullet \tag{2}$$

$$H_2O + V^{\bullet\bullet}_O + 3O^\times_O \rightarrow 2OH^\bullet_O \tag{3}$$

$$H_2 + 2h^\bullet + 2O^\times_O \rightarrow 2OH^\bullet_O \tag{4}$$

In dry air, BCZYSm10 exhibit the mixed electronic and oxygen ionic conductivity. The introduction of water vapor provides a new proton incorporation path because water molecules can react with oxygen vacancy or lattice oxygen (Equation (3)), through which protonic defects can be generated. An enhanced conductivity and decreased activation energy in wet air can be observed as compared to dry air. In wet oxygen, the conductivity is further increased due to the partial pressure dependence of the total conductivity as expressed by: $\sigma_{tot} = a + bp_{O_2}^{1/4}$ [31]. BCZYSm10 exhibits the highest conductivity and lowest activation energy under wet H_2 atmosphere, because the transport properties are predominated by proton conduction which is enhanced in wet atmospheres. Studies on perovskite-type proton conductors showed that contribution of protons to total conductivity decreased as the decrease in proton transport numbers were observed at high temperatures [32,33].

3.3. Performance of RePCEC single cells based on BCZYSm10 electrolyte

In order to further evaluate the electrochemical performance as an electrolyte material, a single cell with thin BCZYSm10 electrolyte was prepared and tested. The SEM image of the cross-sectional morphology of the single cell is shown in Fig. 3. The fully dense electrolyte layer is approximately 25 μm in thickness (Fig. 3b), free of cracks and exhibiting good adhesion to both of the electrode materials .

The electrochemical cell with BCZYSm10 electrolyte has been tested in the reversible proton conducting fuel cell mode of operation (Fig. 4). The I–V curves in the protonic ceramic fuel cell (PCFC) mode were obtained down to 0.5 V, which is sufficient to reach the maximum power density of the cell (P_{max}) at each temperature. The P_{max} value reaches 410 mWcm⁻² at 600 °C and exemplary impedance spectroscopy plots are shown in Fig. S7. The enhancement of output characteristic can be realized through the optimization of electrode microstructures and electrolyte thin film development. The IV curves in the protonic ceramic electrolysis cell (PCEC) mode of operation were obtained, with 12 vol% H_2O humidified air as feed gas and wet H_2 as sweep gas. The cell was also able to produce current density of 370 mAcm⁻² with an applied voltage of 1.3 V at 600 °C. Table 1 summarizes the performance of other reversible proton conducting electrolysis cells in the literature. The performance of the electrolysis cell in this work is lower than the best reported current density due to the different overpotential as well as water vapor pressure in the fed side. The developed cell operating in the PCEC mode possesses encouraging performance in comparison with most of the previously studied systems. It is worth mention that the electrolysis performance can be further enhanced by increasing the water content in the feed stream.

4. Conclusions

In this work, the dopant effects of the electrical conductivity of $BaCe_{0.7}Zr_{0.1}Y_{0.2-x}Sm_xO_{3-\delta}$ proton conductors was studied. Sm-doping was shown to effectively promote the growth of grains and enhance the electrolyte density. The conductivity variation of $BaCe_{0.7}Zr_{0.1}Y_{0.2-x}Sm_xO_{3-\delta}$ polycrystalline was determined by proton mobility and grain/grain boundary conductivity. At 600 °C, $BaCe_{0.7}Zr_{0.1}Y_{0.1}Sm_{0.1}O_{3-\delta}$

Table 1
Summary of the electrolyte, thickness of the electrolyte, cathode materials, and current density for recent RePCESs.

Electrolyte material and thickness (μm)	Cathode	Condition (cathode/anode)	Applied voltage (overvoltage) (V)	Current density (mAcm⁻²)	Ref.
$BaCe_{0.5}Zr_{0.3}Dy_{0.2}O_{3-\delta}$ (25 μm)	$BaCe_{0.5}Zr_{0.3}Dy_{0.2}O_{3-\delta}$	Wet (3%) air/wet (3%) H_2	1.3 (0.4)	178.7 at 600 °C	[34]
$BaZr_{0.9}Y_{0.1}O_{3-\delta}$ (15 μm)	$La_{0.6}Sr_{0.4}Co_{0.2}Fe_{0.8}O_{3-\delta}$-$BaZr_{0.8}Y_{0.2}O_{3-\delta}$	Wet (3%) air/4% H_2 in Ar	1.32 (0.46)	55 at 600 °C	[6]
$BaCe_{0.7}Zr_{0.1}Y_{0.1}Yb_{0.1}O_{3-\delta}$ (20 μm)	BCFZY0.1	85% H_2O humidified air/Ar	1.3 (0.5)	1150 at 600 °C	[7]
$BaCe_{0.5}Zr_{0.3}Y_{0.2}O_{3-\delta}$ (20 μm)	SSC-BZCYY	50% H_2O humidified air	1.5 (0.53)	330 at 600 °C	[35]
$SrZr_{0.5}Ce_{0.4}Y_{0.1}O_{2.95}$ (12 μm)	$Ba_{0.5}La_{0.5}CoO_{3-\delta}$	80% H_2O and 1% O_2	1.63 (0.88)	500 at 600 °C	[36]
$BaCe_{0.7}Zr_{0.1}Y_{0.1}Sm_{0.1}O_{3-\delta}$	BZCY63-BCFZY0.1	12% H_2O humidified air/5% H_2	1.3 (0.3)	370 at 600 °C	This work

possesses largest grain size and exhibited a total conductivity of 7.94×10^{-3} Scm^{-1} at 600 °C, and BaCe$_{0.7}$Zr$_{0.1}$Y$_{0.1}$Sm$_{0.1}$O$_{3-\delta}$ based electrolysis cell was also able to produce current density of 370 mAcm^{-2} with an applied voltage of 1.3 V. This work demonstrated that BaCe$_{0.7}$Zr$_{0.1}$Y$_{0.1}$Sm$_{0.1}$O$_{3-\delta}$ could be utilized as suitable candidates of electrolyte in RePCECs.

Acknowledgement

Appendix A. Supplementary data

Supplementary data to this article can be found online at https://doi.org/10.1016/j.jpowsour.2019.227093.

References

[1] L. Bi, S. Boulfrad, E. Traversa, Steam electrolysis by solid oxide electrolysis cells (SOECs) with proton-conducting oxides, Chem. Soc. Rev. 43 (2014) 8255–8270, https://doi.org/10.1039/C4CS00194J.

[2] Y. Gan, J. Zhang, Y. Li, S. Li, K. Xie, J.T.S. Irvine, Composite oxygen electrode based on LSCM for steam electrolysis in a proton conducting solid oxide electrolyzer, J. Electrochem. Soc. 159 (2012) F763–F767, https://doi.org/10.1149/2.018212jes.

[3] H. Iwahara, H. Uchida, I. Yamasaki, High-temperature steam electrolysis using SrCeO$_3$-based proton conductive solid electrolyte, Int. J. Hydrogen Energy 12 (1987) 73–77, https://doi.org/10.1016/0360-3199(87)90082-6.

[4] P.A. Stuart, T. Unno, J.A. Kilner, S.J. Skinner, Solid oxide proton conducting steam electrolysers, Solid State Ion. 179 (2008) 1120–1124, https://doi.org/10.1016/j.ssi.2008.01.067.

[5] H. Iwahara, Prospect of hydrogen technology using proton-conducting ceramics, Solid State Ion. 168 (2004) 299–310, https://doi.org/10.1016/j.ssi.2003.03.001.

[6] L. Bi, S.P. Shafi, E. Traversa, Y-doped BaZrO$_3$ as a chemically stable electrolyte for proton-conducting solid oxide electrolysis cells (SOECs), J. Mater. Chem. A. 3 (2015) 5815–5819, https://doi.org/10.1039/C4TA07202B.

[7] C. Duan, R. Kee, H. Zhu, N. Sullivan, L. Zhu, L. Bian, D. Jennings, R. O'Hayre, Highly efficient reversible protonic ceramic electrochemical cells for power generation and fuel production, Nature Energy 4 (2019) 230–240, https://doi.org/10.1038/s41560-019-0333-2.

[8] H. Iwahara, H. Uchida, K. Ono, K. Ogaki, Proton conduction in sintered oxides based on BaCeO$_3$, J. Electrochem. Soc. 135 (1988) 529–533.

[9] N. Taniguchi, K. Hatoh, J. Niikura, T. Gamo, H. Iwahara, Proton conductive properties of gadolinium-doped barium cerates at high temperatures, Solid State Ion. 53–56 (1992) 998–1003, https://doi.org/10.1016/0167-2738(92)90283-U.

[10] L. Bi, E. Fabbri, Z. Sun, E. Traversa, BaZr$_{0.8}$Y$_{0.2}$O$_{3-\delta}$-NiO composite anodic powders for proton-conducting SOFCs prepared by a combustion method, J. Electrochem. Soc. 158 (2011) B797–B803, https://doi.org/10.1149/1.3591040.

[11] Z. Shi, W. Sun, Z. Wang, J. Qian, W. Liu, Samarium and yttrium codoped BaCeO$_3$ proton conductor with improved sinterability and higher electrical conductivity, ACS Appl. Mater. Interfaces 6 (2014) 5175–5182, https://doi.org/10.1021/am500467m.

[12] Z. Gong, W. Sun, D. Shan, Y. Wu, W. Liu, Tuning the thickness of Ba-containing "functional" layer toward high-performance ceria-based solid oxide fuel cells, ACS Appl. Mater. Interfaces 8 (2016) 10835–10840, https://doi.org/10.1021/acsami.6b01000.

[13] S. Wang, J. Shen, Z. Zhu, Z. Wang, Y. Cao, X. Guan, Y. Wang, Z. Wei, M. Chen, Further optimization of barium cerate properties via co-doping strategy for potential application as proton-conducting solid oxide fuel cell electrolyte, J. Power Sources 387 (2018) 24–32, https://doi.org/10.1016/j.jpowsour.2018.03.054.

[14] P. Sawant, S. Varma, B.N. Wani, S.R. Bharadwaj, Synthesis, stability and conductivity of BaCe$_{0.8-x}$Zr$_x$Y$_{0.2}$O$_{3-\delta}$ as electrolyte for proton conducting SOFC, Int. J. Hydrogen Energy 37 (2012) 3848–3856, https://doi.org/10.1016/j.ijhydene.2011.04.106.

[15] T. Zhang, J. Ma, L. Kong, S. Chan, J. Kilner, Aging behavior and ionic conductivity of ceria-based ceramics: a comparative study, Solid State Ion. 170 (2004) 209–217, https://doi.org/10.1016/j.ssi.2004.03.003.

[16] S. Kuharuangrong, Ionic conductivity of Sm, Gd, Dy and Er-doped ceria, J. Power Sources 171 (2007) 506–510, https://doi.org/10.1016/j.jpowsour.2007.05.104.

[17] H. Iwahara, Performance of solid oxide fuel cell using proton and oxide ion mixed ConductorsBasedon BaCe$_{1-x}$Sm$_x$O$_{3-\alpha}$, J. Electrochem. Soc. 140 (1993) 1687–1691.

[18] E. Gorbova, V. Maragou, D. Medvedev, A. Demin, P. Tsiakaras, Investigation of the protonic conduction in Sm doped BaCeO$_3$, J. Power Sources 181 (2008) 207–213, https://doi.org/10.1016/j.jpowsour.2008.01.036.

[19] R. Cook, A. Sammells, On the systematic selection of perovskite solid electrolytes for intermediate temperature fuel cells, Solid State Ion. 45 (1991) 311–321, https://doi.org/10.1016/0167-2738(91)90167-A.

[20] K.D. Kreuer, Proton-conducting oxides, Annu. Rev. Mater. Res. 33 (2003) 333–359, https://doi.org/10.1146/annurev.matsci.33.022802.091825.

[21] D. Pergolesi, E. Fabbri, A. D'Epifanio, E. Di Bartolomeo, A. Tebano, S. Sanna, S. Licoccia, G. Balestrino, E. Traversa, High proton conduction in grain-boundary-free yttrium-doped barium zirconate films grown by pulsed laser deposition, Nat. Mater. 9 (2010) 846–852, https://doi.org/10.1038/nmat2837.

[22] F. Iguchi, N. Sata, T. Tsurui, H. Yugami, Microstructures and grain boundary conductivity of BaZr$_{1-x}$Y$_x$O$_3$ (x=0.05, 0.10, 0.15) ceramics, Solid State Ion. 178 (2007) 691–695, https://doi.org/10.1016/j.ssi.2007.02.019.

[23] Z. Sun, E. Fabbri, L. Bi, E. Traversa, Lowering grain boundary resistance of BaZr$_{0.8}$Y$_{0.2}$O$_{3-\delta}$ with LiNO$_3$ sintering-aid improves proton conductivity for fuel cell operation, Phys. Chem. Chem. Phys. 13 (2011) 7692–7700, https://doi.org/10.1039/C0CP01470B.

[24] J. Tong, D. Clark, M. Hoban, R. O'Hayre, Cost-effective solid-state reactive sintering method for high conductivity proton conducting yttrium-doped barium zirconium ceramics, Solid State Ion. 181 (2010) 496–503, https://doi.org/10.1016/j.ssi.2010.02.008.

[25] J. Tong, D. Clark, L. Bernau, A. Subramaniyan, R. O'Hayre, Proton-conducting yttrium-doped barium cerate ceramics synthesized by a cost-effective solid-state reactive sintering method, Solid State Ion. 181 (2010) 1486–1498, https://doi.org/10.1016/j.ssi.2010.08.022.

[26] D. Huan, W. Wang, Y. Xie, N. Shi, Y. Wan, C. Xia, R. Peng, Y. Lu, Investigation of real polarization resistance for electrode performance in proton-conducting electrolysis cells, J. Mater. Chem. A. 6 (2018) 18508–18517, https://doi.org/10.1039/C8TA06862C.

[27] J. Guan, The effects of dopants and A:B site nonstoichiometry on properties of perovskite-type proton conductors, J. Electrochem. Soc. 145 (1998) 1780, https://doi.org/10.1149/1.1838557.

[28] M. Amsif, D. Marrero-Lopez, J.C. Ruiz-Morales, S.N. Savvin, M. Gabás, P. Nunez, Influence of rare-earth doping on the microstructure and conductivity of BaCe$_{0.9}$Ln$_{0.1}$O$_{3-\delta}$ proton conductors, J. Power Sources 196 (2011) 3461–3469, https://doi.org/10.1016/j.jpowsour.2010.11.120.

[29] C. Zhang, H. Zhao, S. Zhai, Electrical conduction behavior of proton conductor BaCe$_{1-x}$Sm$_x$O$_{3-\delta}$in the intermediate temperature range, Int. J. Hydrogen Energy 36 (2011) 3649–3657, https://doi.org/10.1016/j.ijhydene.2010.12.087.

[30] N. Danilov, J. Lyagaeva, A. Kasyanova, G. Vdovin, D. Medvedev, A. Demin, P. Tsiakaras, The effect of oxygen and water vapor partial pressures on the total conductivity of BaCe$_{0.7}$Zr$_{0.1}$Y$_{0.2}$O$_{3-\delta}$, Ionics 23 (2017) 795–801, https://doi.org/10.1007/s11581-016-1961-1.

[31] D.-K. Lim, H.-N. Im, S.-Y. Jeon, J.-Y. Park, S.-J. Song, Experimental evidence of hydrogen–oxygen decoupled diffusion into BaZr$_{0.6}$Ce$_{0.25}$Y$_{0.15}$O$_{3-\delta}$, Acta Mater. 61 (2013) 1274–1283, https://doi.org/10.1016/j.actamat.2012.11.003.

[32] D.-K. Lim, M.-B. Choi, K.-T. Lee, H.-S. Yoon, E.D. Wachsman, S.-J. Song, Non-monotonic conductivity relaxation of proton-conducting BaCe$_{0.85}$Y$_{0.15}$O$_{3-\delta}$ upon hydration and dehydration, Int. J. Hydrogen Energy 36 (2011) 9367–9373, https://doi.org/10.1016/j.ijhydene.2011.04.203.

[33] D.-K. Lim, T.-R. Lee, B. Singh, J.-Y. Park, S.-J. Song, Partial conductivities and chemical diffusivities of multi-ion transporting BaZr$_x$Ce$_{0.85-x}$Y$_{0.15}$O$_{3-\delta}$ (x = 0, 0.2, 0.4 and 0.6), J. Electrochem. Soc. 161 (2014) F991–F1001, https://doi.org/10.1149/2.0341410jes.

[34] J. Lyagaeva, N. Danilov, G. Vdovin, J. Bu, D. Medvedev, A. Demin, P. Tsiakaras, A new Dy-doped BaCeO$_3$–BaZrO$_3$ proton-conducting material as a promising electrolyte for reversible solid oxide fuel cells, J. Mater. Chem. 4 (2016) 15390–15399, https://doi.org/10.1039/C6TA06414K.

[35] F. He, D. Song, R. Peng, G. Meng, S. Yang, Electrode performance and analysis of reversible solid oxide fuel cells with proton conducting electrolyte of BaCe$_{0.5}$Zr$_{0.3}$Y$_{0.2}$O$_{3-\delta}$, J. Power Sources 195 (2010) 3359–3364, https://doi.org/10.1016/j.jpowsour.2009.12.079.

[36] K. Leonard, Y. Okuyama, Y. Takamura, Y.-S. Lee, K. Miyazaki, M.E. Ivanova, W.A. Meulenberg, H. Matsumoto, Efficient intermediate-temperature steam electrolysis with Y : SrZr$_3$–SrCeO$_3$ and Y : BaZrO$_3$–BaCeO$_3$ proton conducting perovskites, J. Mater. Chem. A. 6 (2018) 19113–19124, https://doi.org/10.1039/C8TA04019B.